MTLA 30 (2023) 101858

Contents lists available at ScienceDirect

Materialia

journal homepage: www.elsevier.com/locate/mtla

Full Length Article

Non-contact determination of the viscoelastic properties of agar culture media by Brillouin spectroscopy

B. Esteves [a], A. Rocha [a], M.F. Silva [a,b], J.H. Correia [a,b], J.A. Rodrigues [a,b,*]

[a] CMEMS-UMinho, University of Minho, 4800-058 Guimarães, Portugal
[b] LABBELS-Associate Laboratory, Braga/Guimarães, Portugal

ARTICLE INFO

Keywords:
Agar
Brillouin spectroscopy
Viscoelastic properties
Scattering
Photonics
Biomaterial

ABSTRACT

This study aimed to investigate the potential of Brillouin spectroscopy as a non-contact and real-time tool for measuring the viscoelastic properties of agar culture media and using them to determine the percentages of their different components.

The Brillouin spectrum of media samples with varying concentrations of different components was successfully acquired. A custom-designed refractometer was employed for assessing the refractive index of the gels. The study shows that the Brillouin spectrum and viscoelastic properties of the media vary in dependence on the concentration of their different components in a predictable and controllable way and that the variation is different for each of the additives tested.

This approach has the advantage of correlating to the component percentages, providing a non-contact method for evaluating the evolution of the culture medium in real-time, without disturbing the growth of cells or microorganisms. The results of this study have the potential to encourage the design of new tools and methods targeting the prediction, measuring, and control of agar plate behavior during cell culture. This could include measuring and maintaining optimal humidity conditions for maintaining suitable agar plates for cell culture or monitoring cell growth by measuring the consumption of each substance.

1. Introduction

Cell culture is the process of growing cells in a suitable medium and controlled environment, and has a wide range of applications, such as drug discovery, tissue engineering, biomedical research, and quality control [1–8].

Agar plates, which are Petri dishes filled with a growth medium that has been solidified with agar, are widely used as one of the main mediums for culturing and studying cells [9]. Agar constitutes a family of complex polysaccharides found in the cell walls of some red algae and is widely used as a gelling, thickening, and stabilizing agent [10,11]. Agar cultures are inexpensive and quick to prepare, chemically and physically stable, and provide nutritive support for cell growth [12,13]. They are also prone to drying out over time, requiring the use of special humidity-controlled incubators to maintain the moisture level. As it is a solid-like material, it limits access to real-time information about how the different components are being used, without disturbing cell growth.

Brillouin spectroscopy is a technique that analyzes the inelastic scattering of incident light in a given sample [14,15]. Brillouin scattering occurs from the interaction of light with the collective modes, such as acoustic phonons and magnons, resulting in frequency shifts in the range of 0.1–100 GHz, which correlate to the viscoelastic properties of the material [16].

The analyses of the Brillouin spectra of agar plates allow the extraction of important mechanical properties relating to their viscoelasticity, which can be correlated with the percentages of each component of the gel. The evaluation of the mechanical properties of the cell culture medium can also directly impact how cells behave and engage with it. The higher the stiffness, the harder the cell migration will be, affecting its growth and functioning. On the other hand, if the cell culture medium is softer, it will not provide enough support for cell growth [17,18]. Being a non-contact measurement technique, Brillouin spectroscopy can provide a unique way to determine the viscoelastic properties of the agar plate at any given time without disturbing cell growth, not only on the surface but also below the superficial layer, depending on the growth medium used, since agar gel is mostly transparent [19,20].

In this paper, we have used Brillouin spectroscopy to analyze the

* Corresponding author at: CMEMS-UMinho, University of Minho, 4800-058 Guimarães, Portugal.
E-mail address: jrodrigues@dei.uminho.pt (J.A. Rodrigues).

https://doi.org/10.1016/j.mtla.2023.101858
Received 3 May 2023; Accepted 23 July 2023
Available online 25 July 2023

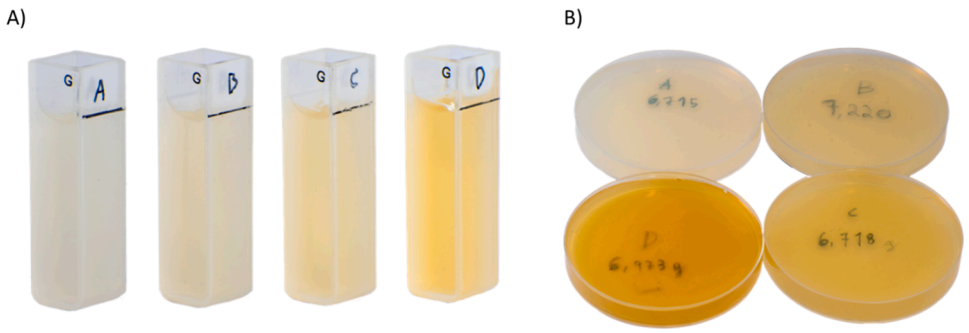

Fig. 1. Agar samples with yeast extract at different concentrations as the additive: A) transparent cuvettes; B) Petri dishes.

viscoelastic properties of agar culture media. The influence on the optical spectrum of some of the most common components used in cell growth media and the possibility of using Brillouin scattering information to determine the composition of each component of the gels were tested. We have also developed a refractometer designed specifically for acquiring the refractive index of agar-based gels, which is necessary for creating viscoelastic models, in addition to acquiring the Brillouin spectrum and measuring density [21].

2. Materials and methods

2.1. Sample preparation

In this study, four different types of agar gel samples were prepared: agar-only, tryptone, yeast extract, and malt extract samples. The agar-only samples were prepared using 7 different target concentrations: 0.5%, 1%, 1.5%, 2%, 2.5%, 3%, and 3.5%. Each sample was prepared by adding the target amount of agar powder (measured using a precision scale) to 60 ml (accounting for approximately 10 ml of evaporation, estimated during the preliminary tests) of distilled water, pre-heated on a hotplate at 120 °C until the water reached between 95 and 97 °C. The mixture was stirred until the agar was completely dissolved and then heated for 15 min. The mixture was then transferred to a pre-weighed and pre-heated glass cuvette (10 mm optical path) and a pre-weighed petri dish and allowed to cool to room temperature (22 °C). The filled cuvette and petri dish were weighed, and the final mass of the gel was determined by subtracting the previously measured empty cuvette and petri dish mass from the sum of their filled mass.

The same procedure was used for the tryptone, yeast extract, and malt extract samples, but with the addition of the corresponding component to the mixture at the same time as the agar powder, both being measured using a precision scale to achieve the desired target concentrations. The target concentrations for tryptone and yeast extract were 0.25%, 0.5%, 1%, and 2%, while for malt extract were 0.5%, 1%, 2%, and 4%. The target amount of agar powder used for these samples was 2%, and 60 ml of distilled water was used for each sample, accounting for approximately 10 ml of evaporation.

The described process was optimized to minimize the effects of water evaporation and other losses on the accuracy of the concentration values of each component, increasing the reliability of the results. For all batches, the required amount of each component was calculated considering approximately 50 ml of water, after evaporation. Following

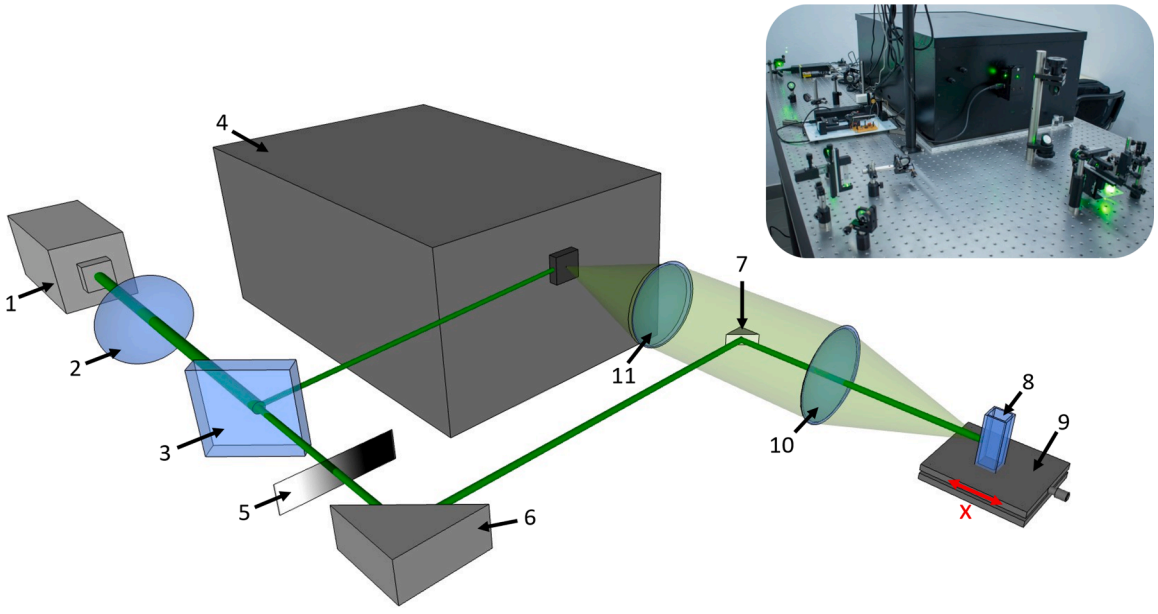

Fig. 2. Optical setup used in the acquisition of the Brillouin spectra. The 532 nm laser light source (1) generates a narrow-collimated beam that passes through a plano-convex lens (2), to avoid beam dispersion, and hits a beamsplitter (3) which sends a small part of the beam to the TFP-2 (4) reference input. The laser light beam then passes through a rectangular continuously variable optical density filter (5), hits the silver mirror (6), which sends it to the small right-angle prism mirror (7) in the backscattering path, and is focused into the sample (8). The focal point on the sample can be adjusted by an x-axis moving platform (9). The sample backscattered light is then gathered by the short focal length collimating lens (10) and focused to the TFP-2 input pinhole by a final gathering lens (11). These lenses must be coaxial and have the same diameter. The diameter (20–30 mm) and focal length (360–400 mm) of the final gathering lens (11) must be chosen so that the light beam fills only the f/18 entrance aperture of the TFP-2 interferometer.

the preparation process, the real concentration of each component was recalculated considering the final mass of the gel produced.

The water heating temperature was chosen to avoid boiling, which accelerates evaporation and premature gel solidification on the walls of the heating container. The cuvettes (Fig. 1A)) provided a transparent and mostly covered container (decreased evaporation) with a known optical path length, ideal for the optical measurement techniques used. Petri dishes (Fig. 1B)) were only used as a container to hold the remaining agar gel from each batch during cooling (needed for measuring its final mass).

All target percentages were based on values commonly used in the literature, while providing enough variation to accurately assess the impact of concentration on the properties being studied. MediaDive, a culture media database that allows for searching growth mediums by components and maximum and minimum concentrations, was used to determine the appropriate values for each component [22].

2.2. Brillouin spectroscopy

A typical Brillouin spectrum is characterized by an intense central peak due to Rayleigh (elastic) scattering and two equally shifted smaller peaks (Brillouin), known as Stokes and Anti-Stokes peaks. The frequency shift of the Brillouin peaks in relation to the Rayleigh peak is denoted by [14]:

$$\omega_B = \pm Vq \tag{1}$$

where V is the acoustic wave velocity in the studied material and q the momentum exchanged in the scattering process [23], which is given by:

$$q = 2nk_i \sin\frac{\theta}{2} \tag{2}$$

where n is the refractive index of the material, θ the scattering angle, and k_i the wave vector of the incident light. The latter depends on the wavelength of incident light in vacuum (λ_i) and is given by:

$$k_i = \frac{2\pi}{\lambda_i} \tag{3}$$

Considering a backscattering geometry, $\theta = 180°$, the momentum equation is simplified:

$$q = 2nk_i \tag{4}$$

Combining the equations given before, the Brillouin peak's frequency shift is equal to:

$$\omega_B = \pm\frac{4\pi n}{\lambda_i} V \tag{5}$$

For a Brillouin scattering experiment, the spectral width of the laser source should be well below the Brillouin linewidth (approximately 1 MHz or less) to avoid spectral broadening of Brillouin peaks and maximize inelastic scattering [15]. The optical setup used for the acquisition of the Brillouin spectra consisted of a 532 nm continuous wave laser (Oxxius L1C-532S), a high-contrast tandem Fabry-Pérot (TFP-2 HC, The Table Stable Ltd) interferometer system, and a custom-built optical mount to send light into the sample and gather the backscattered signal. The full setup is represented in Fig. 2.

The spectrum of each sample was acquired at 3 different points on the agar gel. Laser power at the sample was 50 mW, the focus point was at around 0.5 mm below the agar/glass interface, and for each acquisition, data was acquired until the Brillouin peaks maximum achieved around 1200 cumulative counts on the photodetector (acquisitions of around 10 min).

Brillouin peaks from the resulting spectra were fitted by a Damped Harmonic Oscillator (DHO) function, the theoretically derived expression of the Brillouin line shape of transparent viscoelastic materials acquired at a single q [24,25]. The DHO model used was:

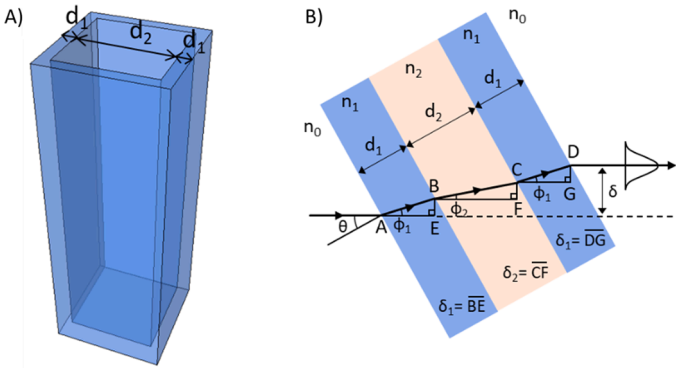

Fig. 3. A) Cuvette used (cell). B) Representation of the displacement of the beam, due to refraction by the cuvette walls and the material in the interior. n_0, n_1 and n_2 represent the refractive index of air, cell walls, and target material, respectively. δ represents the displacement and θ the incident angle.

$$f(\omega) = B + \frac{Io}{2\times\pi} \times \frac{\Gamma_B \times \omega_B^2}{\left(\omega^2 - \omega_B^2\right)^2 + \left(\Gamma_B \times \omega\right)^2} \tag{6}$$

where B is the baseline, Io an intensity arbitrary factor, Γ_B the peak full width at half mean, and ω_B the peak frequency.

2.3. Refractive index measurement

Due to the nature of agar gel, which develops a hard shell through evaporation, there is a potential challenge in obtaining accurate experimental data for determining the percentages of each component using the viscoelastic properties of agar culture media.

The refractive index of the samples was determined using a method described by Shojiro Nemoto [26]. This method uses a transparent cuvette with perfectly parallel walls and a known distance between them, which is filled with the transparent material to be tested. A laser is then impinged obliquely on the container cell, passing through it. The optical path is explained in Fig. 3.

This method is based on a transmission test and uses an optical path that does not contain sample surfaces exposed to the atmosphere. By avoiding the constant surface hardening (due to direct air contact) and testing the entire 10 mm thickness of the sample, we dilute any influence of water evaporation on the sample that could alter the results.

Eqs. (7)–(9) describe how the displacement is dependent on the incidence angle, the cell wall thickness, the distance between the walls, and the refractive index of the walls and the material between them.

$$\delta_i = d_i/(\sin\theta + \cos\theta / \tan\phi_i) \tag{7}$$

$$\phi_i = \theta - \sin^{-1}\left[\left(\frac{n_0}{n_i}\right)\sin\theta\right], i = 1,2 \tag{8}$$

$$\delta_i = d_i\left[1 - \frac{n_0\cos\theta}{\left(n_i^2 - n_0^2\sin^2\theta\right)^{\frac{1}{2}}}\right]\sin\theta$$

$$\delta(n_0,n_1,n_2) = \left\{2d_1\left[1 - \frac{n_0\cos\theta}{\left(n_1^2 - n_0^2\sin^2\theta\right)^{\frac{1}{2}}}\right] + d_2\left[1 - \frac{n_0\cos 0}{\left(n_2^2 - n_0^2\sin^2\theta\right)^{\frac{1}{2}}}\right]\right\}\sin\theta \tag{9}$$

Eqs. (10)–(12) show that by measuring the displacement with an empty cell and again with the filled cell, the difference between the displacements gives the refractive index of the inner material, regardless of cell wall thickness and refractive index.

$$\Delta \equiv \delta(n_0,n_1,n_2) - \delta(n_0,n_1,n_0) \tag{10}$$

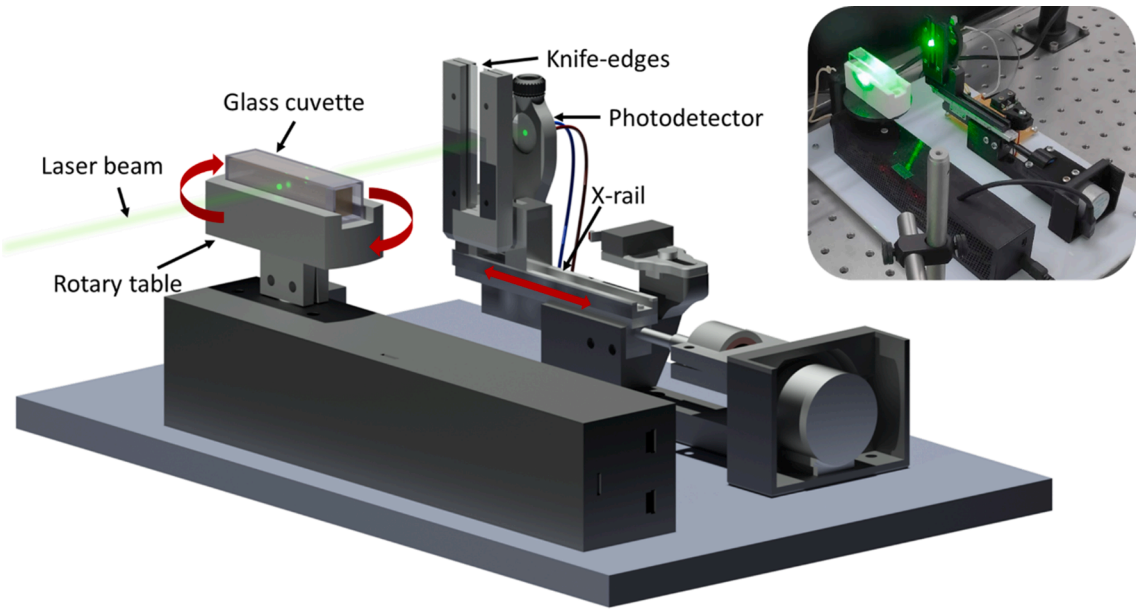

Fig. 4. Refractometer developed for determining the refractive index of agar gel samples.

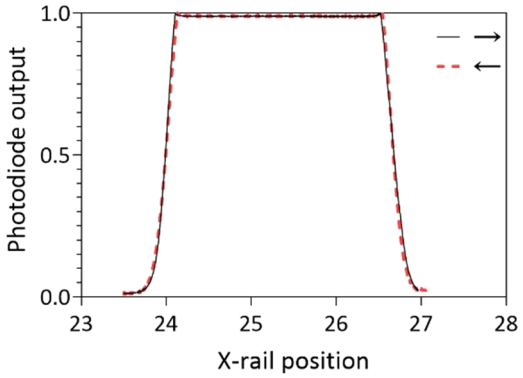

Fig. 5. Representation of the signal obtained from the refractometer (signal from a water sample).

$$\Delta = d_2\left[1-\frac{n_0\cos\theta}{\left(n_2^2-n_0^2\sin^2\theta\right)^{\frac{1}{2}}}\right]\sin\theta \tag{11}$$

$$n_2 = n_0\left\{1+\left[\frac{\cos\theta}{\left(\sin\theta-\frac{\Delta}{d_2}\right)}\right]^2\right\}^{\frac{1}{2}}\sin\theta \tag{12}$$

A custom-made refractometer based on the method described above was developed in order to automate the experiment of accurately determining the refractive index of the samples. Fig. 4 illustrates the developed refractometer.

The refractometer consists of two main parts: the rotary table and the scanning x-rail. The rotary table includes a stepper motor and a support where the cuvette fits perfectly. This table defines the angle between the laser beam and the cuvette, allowing to test several incident angles quickly, sequentially, and accurately. The scanning x-rail consists of a platform that moves perpendicular to the laser beam in only one direction. Combining a stepper motor with an off-the-shelf linear actuator, a resolution of 1.467 μm/step was obtained. On the platform, two knife edges approximately 3 mm apart block all laser light except between them. At the end of the optical path, centered between the two edges, a photodetector was placed to detect the transmitted light. For each angle, the x-rail moves back and forward, creating a plateau with 2 slopes for each pass. An example graph of an acquisition can be seen in Fig. 5.

For measuring the shift between the displacement of an empty cuvette and a filled one, the half-maximum value is considered. However, before calculating this value, the maximum value is corrected by averaging the 50 acquisitions centered on the middle of the plateau, in order to minimize the effect of noise and hysteresis of the acquisition circuit. With a total of 4 slopes for each angle tested, the shift between the displacement of the empty and filled cuvettes is calculated for each of them and averaged.

For each sample, 9 different angles were tested: 20°, 25°, 30°, 35°, 40°, 45°, 50°, 55°, and 60°. Distilled water was used to calibrate the device before testing the agar gel samples. For each sample the acquisition process was repeated passing through 3 different paths by slightly moving the sample in the support, to account for possible inconsistencies within the sample.

2.4. Density measurements

The initial approach for measuring the density of the samples involved filling the cuvettes with agar gel and using the known internal volume and mass of the cuvettes to calculate the gel density. However, this method proved not suitable for agar gel samples due to the uneven surface caused by wall adhesion during the liquid phase and shrinkage during cooling, resulting in inaccuracies. So, in this study, we used an approximation based on a biphasic ideal mixing model. This model accounts for the composition of the gel as a mixture of solid and liquid phases, assuming a uniform distribution of each phase. The mixing model considers the volume fractions of the solid and liquid phases and the corresponding densities of each phase, and can be described by:

$$\rho = \frac{m_w+m_g}{V_w+V_g} = \frac{m_w+m_g}{\frac{m_w}{\rho_w}+\frac{m_g}{\rho_g}} \tag{13}$$

where m_w and m_g correspond to the mass of water and dry components, respectively, and ρ_w and ρ_g are the corresponding mass densities.

Considering a number of solutes greater than 1 (x>1), gel density is approximated to:

$$\rho_A = \frac{m_w + \sum_{i=1}^{x} m_{gi}}{V_w + \sum_{i=1}^{x} V_{gi}} = \frac{m_w + \sum_{i=1}^{x} m_{gi}}{\frac{m_w}{\rho_w} + \sum_{i=1}^{x} \frac{m_{gi}}{\rho_{gi}}} \quad (14)$$

The density of each powdered component was determined using liquid displacement since only the bulk density was provided by the supplier. To ensure that the components would not dissolve during the test, saturated solutions were created for each one and used as the displaced liquid. For each solution, a large amount of the respective component was added to distilled water and mixed for several minutes. The solution was allowed to settle and then decanted and filtered using a 30 μm pore filter. The density of each saturated solution was measured. Finally, in a container of known volume, 3 g of the powder and the respective saturated solution were added until the container was filled (V_T). The density of each component was calculated by:

$$\rho_{gx} = \frac{m_{gx}}{V_T - \frac{m_s}{\rho_s}} \quad (15)$$

2.5. Viscoelastic model

Viscoelasticity represents the elastic and viscous characteristics of a material when undergoing deformation. This dual nature can be described by setting elastic moduli to be complex and frequency-dependent [14,15]. Analysis of the Brillouin spectrum can provide, for a known material density and refractive index, a unique characterization of the material's mechanical properties, because the sound wave properties (such as their velocity or attenuation) exhibit an intrinsic dependence on the viscoelastic properties of the material [21].

The general equation governing the propagation of longitudinal acoustic waves in a viscoelastic medium, the complex longitudinal modulus, M^*, is given by:

$$M^*(\omega) = M'(\omega) + iM''(\omega) \quad (16)$$

where M' is the storage modulus and M'' the loss modulus. The former describes elastic material response to deformation, and the latter refers to energy dissipation due to viscous effects [15].

The storage modulus and loss modulus can be derived from the Brillouin frequency shift ω_B and linewidth Γ_B by [14]:

$$M'(\omega_B) = \frac{\rho}{q^2}\omega_B^2 \quad (17)$$

$$M''(\omega_B) = \frac{\rho}{q^2}\omega_B\Gamma_B \quad (18)$$

Using Eqs. (3) and (4), storage modulus and loss modulus can be rewritten as:

$$M'(\omega_B) = \frac{\rho.\lambda^2.\omega_B^2}{16.n^2.\pi^2} \quad (19)$$

$$M''(\omega_B) = \frac{\rho.\ \lambda^2\omega_B.\Gamma_B}{16.n^2.\pi^2} \quad (20)$$

where λ is the excitation light wavelength (532 nm), and ρ and n are mass density and refractive index of the material, respectively. Eqs. (18) and (19) are valid for backscattering geometry, where the Brillouin shift is expressed in units of angular frequency.

3. Results

3.1. Sample composition

Obtaining agar gel with specific concentrations of each component can be challenging due to water evaporation during the preparation of the sample. Therefore, several target concentrations were defined, considering 16.7% water evaporation during the process.

After cooling to room temperature, the real concentration of each component in the gel was recalculated using the final mass of the sample. The concentrations obtained for each sample are represented on Table 1.

Table 1
Concentrations of each component of the samples.

Culture medium	Sample number	% of agar	% of additive	% of solutes	% of water
Agar (Without additive)	1	0.527	–	0.527	99.473
	2	1.263	–	1.263	98.737
	3	1.606	–	1.606	98.394
	4	2.227	–	2.227	97.773
	5	3.006	–	3.006	96.994
	6	3.011	–	3.011	96.989
	7	3.665	–	3.665	96.335
Agar + tryptone	8	2.019	0.262	2.281	97.719
	9	1.960	0.504	2.463	97.537
	10	1.868	0.973	2.841	97.159
	11	1.858	1.917	3.775	96.225
Agar + yeast extract	12	1.966	0.244	2.210	97.790
	13	2.035	0.496	2.531	97.469
	14	1.891	0.975	2.866	97.134
	15	1.948	1.982	3.930	96.070
Agar + malt extract	16	1.950	0.500	2.450	97.550
	17	2.000	1.001	3.001	96.999
	18	1.915	1.913	3.828	96.172
	19	1.861	3.730	5.591	94.409

3.2. Brillouin scattering

The Brillouin spectrum of the agar gels exhibited a single peak, which is mirrored in the Stokes and anti-Stokes regions. Despite the optical clarity of the medium differed significantly from sample to sample, the effect of multiple scattering (left side of the spectrum) appeared negligible in all of them. This is demonstrated in Fig. 6, which shows one of the samples where this phenomenon is most evident.

Frequency shift and linewidth values were obtained by fitting the Brillouin peaks to the DHO model described in Eq. (6). Fig. 7 shows the frequency shift and linewidth of the Brillouin spectrum of all samples as a function of the mass concentration of the corresponding component. The analysis is straightforward for the samples with only agar and water. However, for samples with additional components, the graph does not represent the amount of agar used. Although the targeted mass concentration of agar was 2%, the actual concentration was found to be 2 +/− 0.139% due to unpredictable water evaporation. The results correlating to water concentration are shown in the discussion chapter. The results revealed an increase in the frequency shift and linewidth with increasing polymer concentration. Although recent proposals

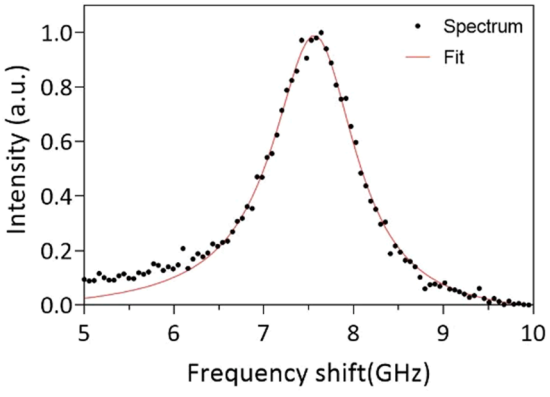

Fig. 6. Example of the anti-Stokes Brillouin peak from the sample with the highest concentration of yeast extract, and the fit using the DHO model.

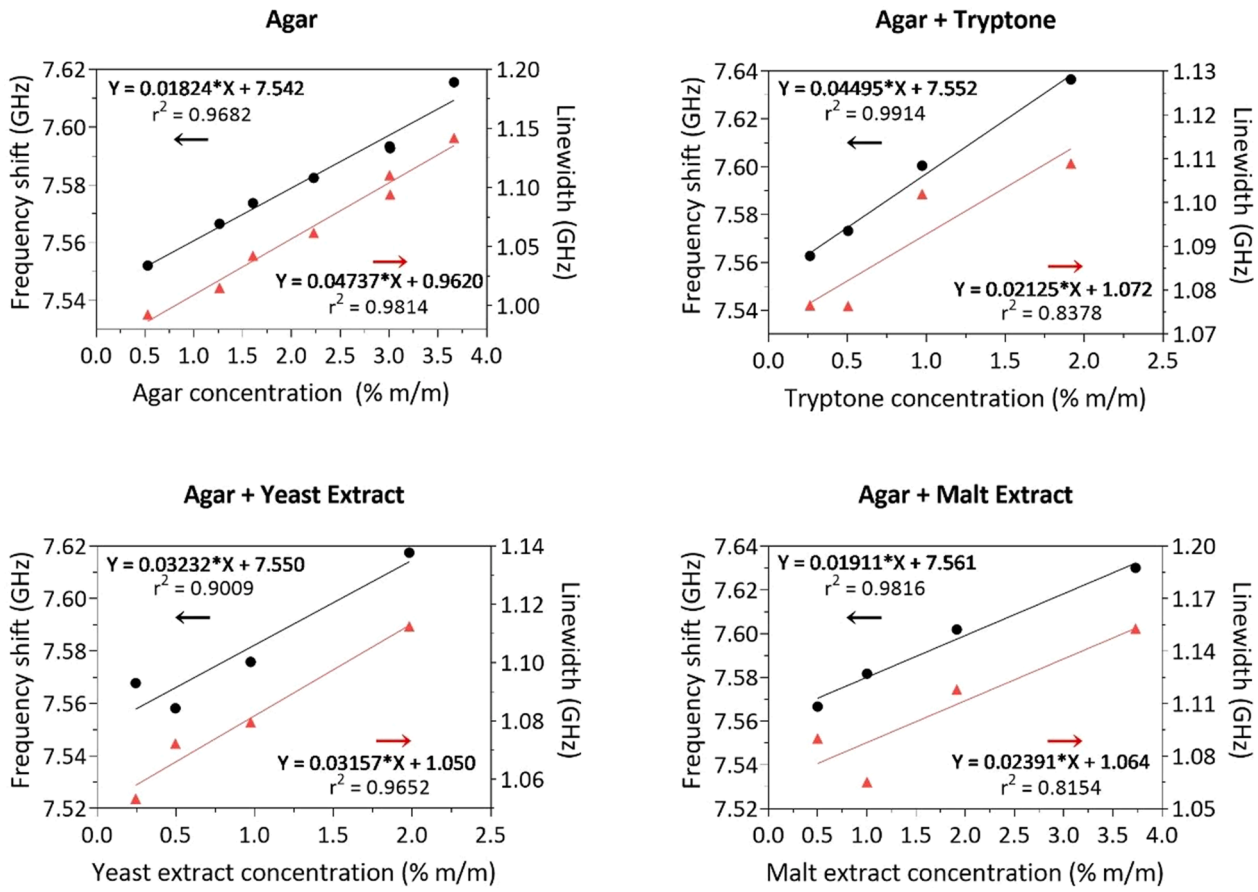

Fig. 7. Frequency shift and linewidth of the Brillouin spectra of all samples as a function of the mass concentration of the component under study.

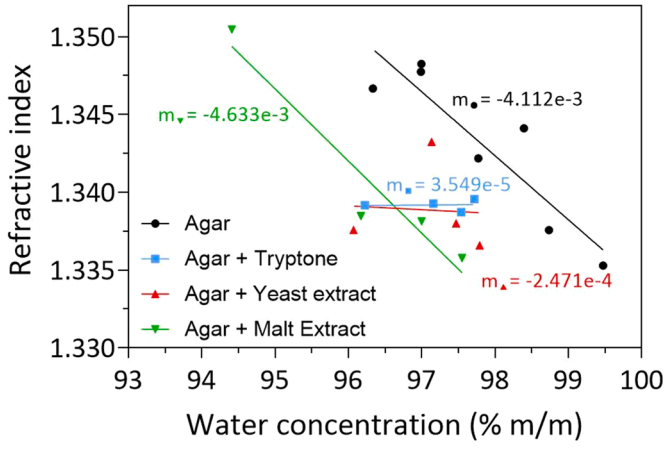

Fig. 8. Refractive index of all samples as a function of the water mass concentration.

Table 2
Density of the saturated solutions and powder solutes.

Material	Saturated solution density (g/ml)	Powder density (g/ml)
Agar	1.0004	1.4022
Tryptone	1.1325	1.9601
Yeast extract	1.1705	1.7702
Malt extract	1.1590	1.6573

suggest that water content primarily influences the Brillouin spectroscopy characteristics of gels, significant differences were observed in agar gels with similar concentrations but different compositions, indicating that the composition of agar gels also plays a significant role in the Brillouin signal.

3.3. *Refractive index*

Although all the samples were prepared using the same protocol, some of the samples resulted in more opaque gels with visible defects (effect particularly prevalent on the ones containing yeast extract). As a transmission method was used for the refractive index calculation, diffraction within the sample heavily impacted the results for the irregular samples. The refractive index obtained for all samples as a function of the water mass concentration is shown in Fig. 8.

It was observed that higher agar concentrations lead to an increase in the refractive index, with values and trend that are similar to those obtained for agarose gels [27]. However distinct behaviors were observed for each additive. The addition of a low concentration of a secondary component was found to slightly reduce the refractive index compared to the 2% agar-only control sample. Increasing malt extract concentration had a similar effect on the refractive index as increasing the agar concentration. On the other hand, adding tryptone had little to no effect on the refractive index, except for the aforementioned reduction. The yeast extract samples exhibited the most noticeable defects on the gels, and the obtained data reflects this, as they showed no discernible trend in refractive index with increasing component concentration.

Since the values obtained for the refractive index were affected by the optical defects present on the gels, in order to mitigate the associated uncertainty when calculating the storage and loss modulus, values

Table 3
Density of each agar sample.

Culture medium	Sample number	Approximated density (g/ml)
Agar (without additive)	1	1.0043
	2	1.0066
	3	1.0066
	4	1.0085
	5	0.9994
	6	1.0015
	7	1.0025
Agar + tryptone	8	1.0050
	9	1.0061
	10	1.0081
	11	1.0128
Agar + yeast extract	12	1.0046
	13	1.0060
	14	1.0077
	15	1.0123
Agar + malt extract	16	1.0055
	17	1.0077
	18	1.0112
	19	1.0185

obtained from the linear regression models shown in Fig. 8 were used instead.

3.4. Density

The results for the density measurements of the saturated solutions and powders solutes are displayed in Table 2.

Additionally, the approximate density values of each agar sample are listed in Table 3. These values were calculated using the biphasic model presented in Eqs. (13) and (14).

3.5. Viscoelastic model

The viscoelastic model described in the methods chapter is reliant on both the refractive index and density of the material. Therefore, errors arising from optical defects of the samples and uncertainties resulting from the density calculation may impact the accuracy of the viscoelastic model presented in this study.

The storage modulus (M′) and loss modulus (M″) were calculated using Eqs. (19) and (20), respectively. Fig. 9 shows the M′ and M″ of all samples as a function of the mass concentration of the corresponding component.

The results revealed an increase in both M′ and M″ for all tested components, albeit at different rates for each component.

4. Discussion

The objective of this study was to evaluate the effectiveness of Brillouin spectroscopy in the real-time determination of viscoelastic properties of agar gels. These properties can help in determining the concentration of individual components in the gel, as well as assess the suitability of the medium for cell growth. In order to establish a viscoelastic model for Brillouin spectroscopy, the Brillouin spectrum, refractive index, and density of the agar gels were analyzed.

Brillouin spectra of the agar gels exhibited a single Stokes and anti-Stokes peak. The frequency shift and linewidth values were obtained

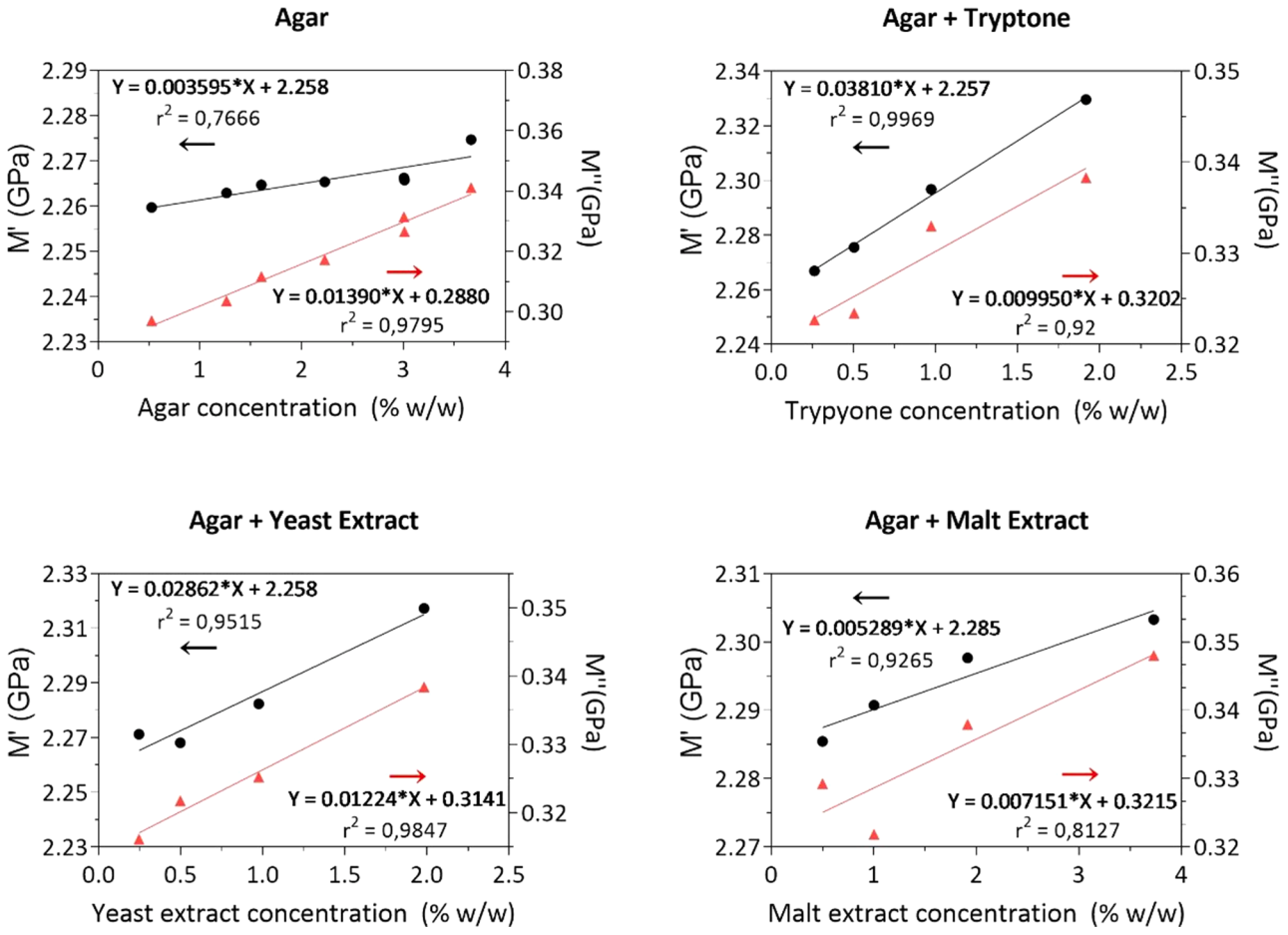

Fig. 9. Storage and loss modulus for all samples as a function of the mass concentration of the component under study.

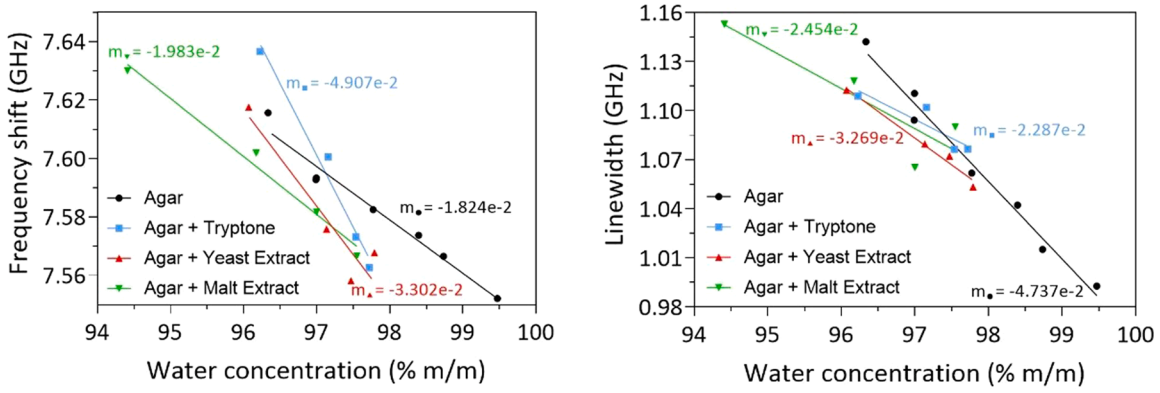

Fig. 10. Brillouin shift and linewidth of all samples as a function of the water mass concentration.

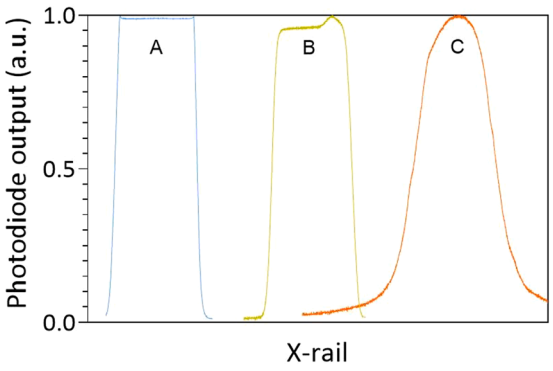

Fig. 11. Representation of the signal acquired using the custom-built refractometer for a: A) cuvette filled with water; B) cuvette filled with agar gel containing only water and agar; C) cuvette filled with agar gel containing the highest concentration of yeast extract tested.

by fitting the peaks to the DHO model, as described in Eq. (6). The results revealed that an increase in agar concentration leads to an increase in both frequency and linewidth. Furthermore, when the agar concentration remained constant and the additive concentration was increased, a similar trend was observed, regardless of the type of additive. To illustrate this relationship, Fig. 10 shows the Brillouin shift and linewidth as a function of the water mass concentration.

Recent studies propose that the Brillouin spectroscopy characteristics of gels are mainly affected by the water content [28], which by itself could be a useful property to determine using Brillouin spectroscopy, since a non-contact and real-time measurement of water concentration could be implemented in incubators to better control the agar suitability for cell growth. Despite that, the clear differences present in gels of similar concentration and different compositions indicate that the composition of agar gels can have an impact on the Brillouin signal of agar gels.

Our results indicate that low concentrations of additives in the agar gels can lower the frequency shift relative to a gel made with only agar and water at the same solute concentration. As the concentration of additives increases, the Brillouin shift also increases, although at different rates depending on the type of additive (Fig. 10). In terms of linewidth, low concentrations of additives do not seem to have a significant effect. However, at higher concentrations, the increase in linewidth is slower compared to agar gels containing only water and agar.

The refractive index was investigated using a custom-built refractometer that was specifically designed for this study. Although the refractometer was intended to provide high accuracy for samples that would suffer from water evaporation on exposed surfaces, the transmission method presented some challenges. The agar gels obtained showed varying levels of transparency, and some had prevalent defects that visibly widened the laser beam during the experiment. A comparison of the data obtained for different samples is shown in Fig. 11.

As depicted in the graph, the transparency of the agar gels containing only water and agar results in two clear and distinct slopes, similar to those obtained from distilled water. However, the addition of yeast extract seems to have a significant impact on the transparency, leading to poorly defined asymmetric slopes and plateau. This effect significantly affected the accuracy of the results, as demonstrated in Fig. 8. The impact of yeast extract on the refractive index does not show a clear trend, probably due to the poor-quality data caused by the defects in the samples. Nonetheless, for all additives tested, low concentrations seem to decrease the refractive index compared to gels composed only of water and agar. Malt extract, in particular, does not show any significant additional effect on the refractive index, while increasing the agar concentration or adding malt extract provides a similar increase.

Although surface reflection is the ideal method for obtaining the refractive index of an agar plate without disturbing growth, a transmission method is preferable for creating a precise correlation with the concentrations of the agar constituents. We also investigated the effect of the maximum heating temperature on the optical defects of agar gels with yeast extract as an additive and found that increasing the temperature can mitigate these defects. Adjusting the agar medium recipe could be a potential solution to this issue, although it poses the risk of premature agar solidification on the heating container walls and a more significant effect of water evaporation on the final component concentration.

The biphasic model used for the density approximation of the agar gel samples has limitations and may not provide the same level of accuracy as direct measurement. However, it allowed us to obtain a reasonable approximation of the agar density. The direct density measuring techniques available were not practical due to issues such as wall adhesion while the agar was liquid, uneven shrinking during cooling, and rapid water evaporation. Obtaining accurate real-time density measurements on agar plates without disturbing cell growth would be challenging. In addition to evaporation, the larger consumption of agar components by cells on the surface could create a density gradient, making it difficult to obtain accurate measurements using techniques such as X-ray, gamma-ray, or ultrasound densitometry. Future studies could explore alternative methods for estimating density in agar plates, such as ellipsometry or other surface thickness measurement techniques, which could potentially provide more accurate and real-time measurements. However, given the challenges associated with the agar matrix, such as its tendency to form density gradients, the use of approximation-based approaches remains necessary in some cases.

The storage and loss moduli were calculated using Eqs. (19) and (20),

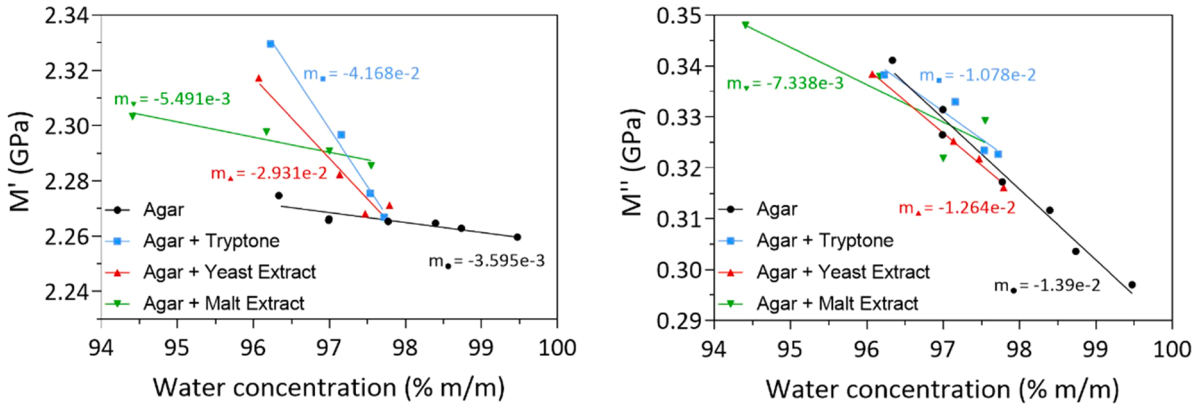

Fig. 12. Storage modulus (M′) and loss modulus (M″) of all samples as a function of the water mass concentration.

respectively. Fig. 12 shows the storage and loss moduli of all samples as a function of the water mass concentration.

Distinct trends can be observed in the storage modulus, depending on the type of additive added, while the loss modulus seems more dependent on the water content.

In summary, this study shows that the mechanical properties of agar gels can be significantly influenced by the inclusion of common additives. The refractive index, density, Brillouin spectrum, and viscoelastic properties were found to be dependent on the composition of the agar gels, providing insight into the design of culture mediums with optimal mechanical properties for cell growth. Furthermore, the study results may inform the development of real-time and non-invasive monitoring technologies for culture media, enabling the evaluation of cell multiplication and propagation.

5. Conclusions

This study explored the application of Brillouin spectroscopy in assessing the viscoelastic properties of agar culture media containing different concentrations of some of the most common components. Gels with different concentrations of agar, tryptone, yeast extract, and malt extract were tested. The Brillouin spectrum and refractive index of all samples were measured, and the biphasic model was used to approximate density. Based on these properties, the storage and loss moduli were then calculated.

A custom-designed refractometer was employed to determine the refractive index of the gels. The refractometer was optimized to address the challenges associated with obtaining accurate measurements in a gel with a constantly hardening surface due to water evaporation.

This study revealed that the viscoelastic properties of agar culture media are dependent on the percentage of each component, and that the variation of the concentration of each one results in distinct changes in the Brillouin spectrum.

The accuracy of the viscoelastic model may be improved further by refining the experimental setup for measuring the refractive index, optimizing the agar gel protocol, and improving density measuring.

In conclusion, our findings provide important insights into the development of culture media with optimal mechanical properties for cell growth and development of real-time and non-invasive tools for monitoring the culture medium during cell growth and propagation.

Declaration of Competing Interest

The authors declare that they have no known competing financial interests or personal relationships that could have appeared to influence the work reported in this paper.

Data availability

The original contributions presented in the study are included in the article further inquiries can be directed to the corresponding author/s.

Acknowledgments

This work was supported by CMEMS-UMinho Strategic Project UIDB/04436/2020 and UIDP/04436/2020 and project MPhotonBiopsy, PTDC/FIS-OTI/1259/2020. Bruno Esteves was supported by FCT, PhD grant 2021.07239.BD.

References

[1] K. Duval, H. Grover, L.H. Han, Y. Mou, A.F. Pegoraro, J. Fredberg, Z. Chen, Modeling physiological events in 2D vs. 3D cell culture, Physiology 32 (2017) 266–277, https://doi.org/10.1152/physiol.00036.2016.
[2] D. Anton, H. Burckel, E. Josset, G. Noel, Three-dimensional cell culture: a breakthrough in vivo, Int. J. Mol. Sci. 16 (2015) 5517–5527, https://doi.org/10.3390/ijms16035517.
[3] W.L. Mckeehan, D. Barnes, L. Reid, E. Stanbridge, H. Murakami, G.H. Sato, Frontiers in mammalian cell culture, In vitro Cell. Dev. Biol. 26 (1990) 9–23, https://doi.org/10.2307/4296384.
[4] M. Kapałczyńska, T. Kolenda, W. Przybyła, M. Zajączkowska, A. Teresiak, V. Filas, M. Ibbs, R. Bliźniak, Ł. Łuczewski, K. Lamperska, 2D and 3D cell cultures – a comparison of different types of cancer cell cultures, Arch. Med. Sci. 14 (2018) 910–919, https://doi.org/10.5114/aoms.2016.63743.
[5] R. Edmondson, J.J. Broglie, A.F. Adcock, L. Yang, Three-dimensional cell culture systems and their applications in drug discovery and cell-based biosensors, Assay Drug Dev. Technol. 12 (2014) 207–218, https://doi.org/10.1089/adt.2014.573.
[6] N.K. Inamdar, J.T. Borenstein, Microfluidic cell culture models for tissue engineering, Curr. Opin. Biotechnol. 22 (2011) 681–689, https://doi.org/10.1016/j.copbio.2011.05.512.
[7] K. Ng, B. Gao, K.W. Yong, Y. Li, M. Shi, X. Zhao, Z. Li, X.H. Zhang, B. Pingguan-Murphy, H. Yang, F. Xu, Paper-based cell culture platform and its emerging biomedical applications, Mater. Today 20 (2017) 32–44, https://doi.org/10.1016/j.mattod.2016.07.001.
[8] W. Sommeregger, B. Sissolak, K. Kandra, M. von Stosch, M. Mayer, G. Striedner, Quality by control: towards model predictive control of mammalian cell culture bioprocesses, Biotechnol. J. 12 (2017), https://doi.org/10.1002/biot.201600546.
[9] K. Phelan, K.M. May, Basic techniques in mammalian cell tissue culture, Curr. Protoc. Cell Biol. 2015 (2015) 1.1.1–1.1.22, https://doi.org/10.1002/0471143030.cb0101s66.
[10] W.K. Lee, Y.Y. Lim, A.T.C. Leow, P. Namasivayam, J.O. Abdullah, C.L. Ho, Factors affecting yield and gelling properties of agar, J. Appl. Phycol. 29 (2017) 1527–1540, https://doi.org/10.1007/s10811-016-1009-y.
[11] W.J. Chi, Y.K. Chang, S.K. Hong, Agar degradation by microorganisms and agar-degrading enzymes, Appl. Microbiol. Biotechnol. 94 (2012) 917–930, https://doi.org/10.1007/s00253-012-4023-2.
[12] N. Gupta, V. Jain, M.R. Joseph, S. Devi, A review on micropropagation culture method, Asian J. Pharm. Res. Dev. 8 (2020) 86–93, https://doi.org/10.22270/ajprd.v8i1.653.
[13] K.B. Guiseley, Chemical and physical properties of algal polysaccharides used for cell immobilization, Enzyme Microb. Technol. 11 (1989) 706–716, https://doi.org/10.1016/0141-0229(89)90119-1.
[14] F. Palombo, D. Fioretto, Brillouin light scattering: applications in biomedical sciences, Chem. Rev. 119 (2019) 7833–7847, https://doi.org/10.1021/acs.chemrev.9b00019.

[15] C. Poon, J. Chou, M. Cortie, I. Kabakova, Brillouin imaging for studies of micromechanics in biology and biomedicine: from current state-of-the-art to future clinical translation, J. Phys. Photonics 3 (2021) 1–24, https://doi.org/10.1088/2515-7647/abbf8c.
[16] F. Scarponi, S. Mattana, S. Corezzi, S. Caponi, L. Comez, P. Sassi, A. Morresi, M. Paolantoni, L. Urbanelli, C. Emiliani, L. Roscini, L. Corte, G. Cardinali, F. Palombo, J.R. Sandercock, D. Fioretto, High-performance versatile setup for simultaneous Brillouin-Raman microspectroscopy, Phys. Rev X 7 (2017) 1–11, https://doi.org/10.1103/PhysRevX.7.031015.
[17] A. Aygan, B. Arikan, An overview on bacterial motility detection, Int. J. Agric. Biol. 9 (2007) 193–196. http://www.fspublishers.org.
[18] S. Zheng, M. Bawazir, A. Dhall, H.E. Kim, L. He, J. Heo, G. Hwang, Implication of surface properties, bacterial motility, and hydrodynamic conditions on bacterial surface sensing and their initial adhesion, Front. Bioeng. Biotechnol. 9 (2021) 1–22, https://doi.org/10.3389/fbioe.2021.643722.
[19] C. Handler, G. Scarcelli, J. Zhang, Time-lapse mechanical imaging of neural tube closure in live embryo using Brillouin microscopy, Sci. Rep. 13 (2023) 1–8, https://doi.org/10.1038/s41598-023-27456-z.
[20] G. Antonacci, S. Braakman, Biomechanics of subcellular structures by non-invasive Brillouin microscopy, Sci. Rep. 6 (2016) 1–7, https://doi.org/10.1038/srep37217.
[21] R. Prevedel, A. Diz-Muñoz, G. Ruocco, G. Antonacci, Brillouin microscopy: an emerging tool for mechanobiology, Nat. Methods 16 (2019) 969–977, https://doi.org/10.1038/s41592-019-0543-3.
[22] J. Koblitz, P. Halama, S. Spring, V. Thiel, C. Baschien, R.L. Hahnke, M. Pester, J. Overmann, L.C. Reimer, MediaDive: the expert-curated cultivation media database, Nucleic Acids Res. 51 (2023) D1531–D1538, https://doi.org/10.1093/nar/gkac803.
[23] M. Pochylski, J. Gapiński, Simple way to analyze Brillouin spectra from turbid liquids, Opt. Lett. 40 (2015) 1456, https://doi.org/10.1364/ol.40.001456.
[24] M. Mattarelli, G. Capponi, A.A. Passeri, D. Fioretto, S. Caponi, Disentanglement of multiple scattering contribution in Brillouin microscopy, ACS Photonics 9 (2022) 2087–2091, https://doi.org/10.1021/acsphotonics.2c00322.
[25] S. Mattana, M. Mattarelli, L. Urbanelli, K. Sagini, C. Emiliani, M.D. Serra, D. Fioretto, S. Caponi, Non-contact mechanical and chemical analysis of single living cells by microspectroscopic techniques, Light Sci. Appl. 7 (2018) 1–9, https://doi.org/10.1038/lsa.2017.139.
[26] S. Nemoto, Measurement of the refractive index of liquid using laser beam displacement, Appl. Opt. 31 (1992) 6690, https://doi.org/10.1364/ao.31.006690.
[27] E. Fujiwara, T.D. Cabral, M. Sato, H. Oku, C.M.B. Cordeiro, Agarose-based structured optical fibre, Sci. Rep. 10 (2020) 1–8, https://doi.org/10.1038/s41598-020-64103-3.
[28] P.J. Wu, I.V. Kabakova, J.W. Ruberti, J.M. Sherwood, I.E. Dunlop, C. Paterson, P. Török, D.R. Overby, Water content, not stiffness, dominates Brillouin spectroscopy measurements in hydrated materials, Nat. Methods 15 (2018) 561–562, https://doi.org/10.1038/s41592-018-0076-1.